AIAA JOURNAL
Vol. 47, No. 3, March 2009

Asymptotic Solutions for Low-Magnetic-Reynolds-Number Gas Flows Inside a Two-Dimensional Channel

Chunpei Cai*
New Mexico State University, Las Cruces, New Mexico 88003
and
Danny D. Liu†
ZONA Technology, Inc., Scottsdale, Arizona 85258

DOI: 10.2514/1.37060

This paper analyzes a near-continuum compressible magneto-gas-dynamic flow inside a two-dimensional microchannel or a two-dimensional channel of conventional dimensions, with a low-magnetic-Reynolds-number assumption. This work represents an extension from the classical Hartmann flow in a two-dimensional channel of infinite length to a microchannel of finite length. First, by comparing the magnitudes of different forces in the compressible gas flow, we obtain a nondimensional *X* momentum equation that relates the pressure ratio, Reynolds number, Mach number, magnetic Reynolds number, and magnetic force number. Second, for two cases of selected nondimensional parameters of comparable magnitude, we solve for asymptotic solutions of velocities, pressure, temperature, and mass flow rate of compressible gas flow based on the velocity-slip and temperature-jump wall boundary conditions while maintaining a consistent quasi-isothermal assumption. It is found that even with a small magnetic Reynolds number, the electric and magnetic field effects on the flow properties can be significant. Numerical solutions of the same formulation are obtained for validation of the present analytical solutions. The major work in this study is theoretical and the solutions are obtained in closed forms that can provide physical insights into flows inside a microchannel or a channel of conventional dimensions.

Nomenclature

B	=	magnetic field strength
D	=	atomic diameter
d	=	channel semiheight
E	=	electric field strength
Ha	=	Hartmann number, $\sqrt{ReR_\sigma R_b}$
K	=	$-E/(u_o B_0)$
Kn	=	Knudsen number
k	=	Boltzmann constant, or thermal conductivity coefficient
L	=	channel length
Ma	=	Mach number based on averaged properties at the outlet, $u_o/\sqrt{\gamma RT_o}$
n	=	number density
P	=	inlet and outlet pressure ratio, p_i/p_o
Pr	=	Prandtl number
p	=	pressure
Q	=	mass flow rate or magnetic interaction factor, $R_\sigma R_b$
R	=	universal gas constant
Re	=	Reynolds number based on averaged properties at the outlet, $\rho_o u_o (2d)/\mu$
R_b	=	magnetic force number, $B_0^2/(\rho_o U_o^2 \mu_m)$
R_σ	=	magnetic Reynolds number, $(2d)U_o \mu_o \sigma_o$
T	=	temperature
U	=	average velocity
u, v, w	=	velocity components
ϵ	=	height-to-length ratio, $2d/L$
γ	=	specific heat ratio
λ	=	mean free path
μ	=	gas viscosity
μ_m	=	magnetic permeability
ρ	=	density
σ	=	electric conductivity
σ_T	=	energy accommodation coefficient
σ_u	=	momentum accommodation coefficient
Θ_T	=	coefficient, $(2-\sigma_T)/\sigma_T$
Θ_u	=	coefficient, $(2-\sigma_u)/\sigma_u$

Subscripts

i, o	=	averaged inlet and outlet properties
w	=	wall property

Received 8 February 2008; accepted for publication 18 December 2008.

*Assistant Professor, Department of Mechanical and Aerospace Engineering, P.O. Box 30001, Department 3450; ccai@nmsu.edu. Senior Member AIAA.

†President; Professor Emeritus, Arizona State University, 9489 East Ironwood Square Drive. Fellow AIAA.

I. Introduction

MICROCHANNELS are important components for many microelectromechanical systems, and it has been an interesting research topic to study gaseous flows inside microchannels. In the literature, there are many reports about gas flows in microchannels and microtubes [1–5]. A microchannel for fuel cells, for example, is of the dimensions of micrometers, whereas a channel of conventional dimensions is on the order of centimeters to meters. It is well accepted that for near-continuum gas flows through microchannels, the Navier–Stokes equations are valid if a slip wall boundary condition is used. Many researchers have obtained theoretical solutions for the flow distributions along a microchannel with an isothermal assumption: for example, the pioneering work by Arkilic et al. [5], Karniadakis and Beskok [6], and Zohar et al. [7]. Numerically, there are many simulations of compressible flows in a microchannel as well: for example, with the direct simulation Monte Carlo method [8–10], the information-preservation method [11,12], the direct methods for solving the Boltzmann equation [13], the method on the basis of the linearized Boltzmann equations [14], and gas-kinetic Bhatnagar–Gross–Krook–Burnett equation solutions [15]. Discussions of thermal heating effects are reported as well [16–20]. Extensive studies have also been carried out on electro-osmotic flows [21] in microchannels in the presence of a pressure

gradient and an electric field. For example, there are studies on a single conducting fluid with zeta potentials at the channel walls [22–26] and two immiscible fluids in a microchannel [27,28].

One important and interesting problem related to gaseous flow inside a microchannel is conductive gas flows under the influence of external magnetic and electric fields or magneto-gas-dynamic (MGD) flows. The magnetic and electric fields can significantly affect the flowfield inside a channel, whereas different placements of electric field enable the channel to perform as a generator, a pump, a flux meter, or an accelerator [29].

We present a study of rarefied gas flow in microchannels with MGD effects. It is an extension of the classical Hartmann flow [29] to a flow in a microchannel of finite length, which could be a continuum or a rarefied gas with a set of general velocity-slip and temperature-jump wall boundary conditions. Gas flow in a channel of conventional dimensions with the same dimension ratio is a special case of such microchannel flows, but with nonslip and constant-temperature wall boundary conditions. Thus, the microchannel flow solutions can revert to those for gas flows inside channels of conventional dimensions. However, this problem differs from the Hartmann flow problem in several aspects. First, for pressure-driven gas flows inside a microchannel, there are usually large density changes inside the microchannel, and the average velocity cannot remain unchanged to maintain a constant mass flow rate. Hence, the invariant-velocity profile from Hartmann flow does not exactly apply here. Second, the boundary conditions are different. For Hartmann flow, there is essentially no variation in the flow direction; wall boundary conditions are nonslip and constant temperature, and at the inlet and outlet, one can use periodic boundary conditions (except for pressure). However, for microchannel flows with density variations and rarefication effects, we will not use periodic boundary conditions at the inlet and outlet; further, we will specify a set of general velocity-slip and temperature-jump wall boundary conditions, which include the continuum nonslip and temperature boundary conditions as a special case. Third, the pressure gradient inside a microchannel of finite length is not assumed to be constant throughout. Simply taking a linear pressure distribution assumption (after the Hartmann flow) for the present microchannel flow will result in solution inaccuracy. Nonetheless, the present microchannel approach tolerates these differences; we will show that our microchannel solutions are indeed related to the Hartmann flow solutions.

The work in this paper is a natural extension from two previous works. The work of Arkilic et al. [5] provided detailed steps to obtain a set of asymptotic solutions for neutral (non-MGD)gas flows inside a microchannel with an isothermal assumption. The work of Cai et al. [20] provided some further improvements on such neutral-gas flows, including estimations for orders of magnitude for the Reynolds and Mach numbers, a quasi-isothermal assumption, a temperature solution, and solutions for gas flow inside a circular microtube. Along the same vein, the present study follows Cai et al.'s [20] previous approach for treatments of microchannel MGD flows. A few works appeared in recent years in the same area of MGD microchannel flow [30,31]. We note the differences between the present approach and others in the following aspects:

1) Our study includes a governing equation for temperature, which is necessary for this study due to the Joule heating effects, and we obtain the temperature field based on the quasi-isothermal assumption [20]; by comparison, the past work neglects the energy equation and adopts the isothermal assumption.

2) We explicitly use the low-magnetic-Reynolds-number assumption, which is crucial to simplify the MGD equations, and we have not noticed any previous treatment for the same problem in the literature. Without this assumption, the magnetic field variations in general should be considered; thus, it is unlikely that such an asymptotic approach can be consistently formulated and that its solutions can be so obtained.

3) According to our X momentum equation, we provide the governing relation between the Re and Ma numbers and two other nondimensional parameters for magnetic and electric fields. We then conducted a consistent order-of-magnitude analysis on a treatment of the X momentum equation, yielding a class of physically meaningful asymptotic solutions. This unique treatment is essential, for it is a crucial step leading to the simplification of the valid MGD microchannel equations adopted presently.

4) We have obtained velocity components U and V, temperature, and pressure distributions in a microchannel MGD flow as a part of the total asymptotic solutions. Our formulation is largely different from the previous U-velocity solution formulation. The nonlinear pressure solution implies that the solution for U velocity would be incorrect without it. This is because the nonlinear pressure gradient is interactively coupled in the equations with velocity components and temperature. It is inappropriate to arbitrarily assume a linear pressure distribution throughout the channel or to substitute numerical nonlinear pressure distribution in the equations for asymptotic solutions.

We remark that (based on points 2 and 3) our solutions for MGD microchannel flow are limited to low magnetic Reynolds numbers, whereas they are invalid with very large Hartmann numbers. This is because an MGD flow with large Hartmann numbers will likely result in strong Joule heating, thus defying the quasi-isothermal flow assumption. Therefore, one questions if it is physically justifiable in a previous work to adopt a large-Hartmann-number flow case for validation of an isothermal-based U-velocity result. Clearly, the difference between our previous work [20] and the present work is the MGD consideration and its low-magnetic-Reynolds-number assumption. With this assumption, the MGD equations revert to Navier–Stokes equations with two extra source terms, accounting for the effects from the electric and magnetic fields. Essentially, this assumption releases one from the heavy burden of solving the magnetic field equations. In so doing, we worked out the present MGD flow solutions in microchannels for small Hartmann numbers, consistent with the quasi-isothermal assumption, and supported by combined external electric and magnetic fields.

This paper is organized as follows: Section II presents the problem, the assumptions used in this study, and the governing equations. Section III estimates the orders of magnitude for different forces in the flowfield. Section IV provides a set of asymptotic solutions to this problem. Section V presents numerical simulation results to validate the asymptotic solutions. Section VI presents conclusions.

II. Problem Description and Governing Equations

As illustrated by Fig. 1, a microchannel has a height of $2d$ and a length of L, and the average compressible gas properties of pressure, density, velocity, and number density are p_o, ρ_o, U_o, and n_o at the channel outlet. The averaged outlet quantities are adopted to normalize the following governing equations and boundary conditions. The inlet pressure is several times larger than the outlet pressure, and the pressure ratio is denoted as P. The coordinate origin is set at the inlet center point, the X axis is along the channel centerline, and the Y axis is along the direction normal to the channel wall.

Assumptions used in this study are as follows:

1) The external magnetic field is fixed at a value B_0 along the Y direction only.

2) The flow is not isothermal, but can be well approximated with a quasi-isothermal assumption [20]. If P is not very large and the Joule heating effects are not strong, this assumption is reasonable.

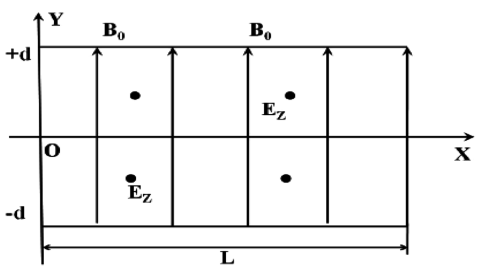

Fig. 1 Illustration of the problem, $B = (0, B_0, 0)$ and $E = (0, 0, E_z)$.

3) Directly based on the preceding assumption, gas viscosity μ, thermal conductivity k, magnetic permeability μ_m, and electric conductivity σ are treated as constants.

4) The magnetic Reynolds number $R_\sigma = (2d)U_o\mu_o\sigma$ is very small. It renders a negligible induced magnetic field B_x when compared with the external magnetic field B_0.

5) The flow is two-dimensional; hence, $\partial/\partial z = 0$ and $w = 0$.

6) The constant external electric field is along the Z direction only, and $E_x = E_y = 0$. Further, we assume that the electric field is linked with the magnetic field with $E_z = -Ku_oB_0$, and $0 < K < 1$ [32]. Hence, in the next section, to estimate orders of magnitude for different forces, we can combine the electric field into the magnetic field.

7) The channel is not short, which means that $\epsilon = 2d/L$ is small. We use this small parameter ϵ to proceed with the analysis.

The corresponding MGD equations for two-dimensional, steady, compressible gas flows with a low magnetic Reynolds number degenerate to the Navier–Stokes equations with two extra source terms [32]:

$$\frac{\partial(\rho u)}{\partial x} + \frac{\partial(\rho v)}{\partial y} = 0 \tag{1}$$

$$\frac{\partial(\rho u^2 + p)}{\partial x} + \frac{\partial(\rho uv)}{\partial y} = \frac{\partial \tau_{xx}}{\partial x} + \frac{\partial \tau_{xy}}{\partial y} - \sigma B_0(E_z + uB_0) \tag{2}$$

$$\frac{\partial(\rho uv)}{\partial x} + \frac{\partial(\rho v^2 + p)}{\partial y} = \frac{\partial \tau_{yx}}{\partial x} + \frac{\partial \tau_{yy}}{\partial y} \tag{3}$$

$$\begin{aligned}&\frac{\partial}{\partial x}\left[\frac{\gamma pu}{\gamma - 1} + \frac{\rho(u^2 + v^2)u}{2}\right] + \frac{\partial}{\partial y}\left[\frac{\gamma pv}{\gamma - 1} + \frac{\rho(u^2 + v^2)v}{2}\right] \\ &\quad = \frac{\partial}{\partial x}(u\tau_{xx} + v\tau_{xy}) + \frac{\partial}{\partial y}(u\tau_{xy} + v\tau_{yy}) \\ &\quad + k\left(\frac{\partial^2 T}{\partial x^2} + \frac{\partial^2 T}{\partial y^2}\right) + \sigma E_z(E_z + uB_0)\end{aligned} \tag{4}$$

$$p = \rho RT \tag{5}$$

where

$$\tau_{xx} = \frac{2}{3}\mu\left(2\frac{\partial u}{\partial x} - \frac{\partial v}{\partial y}\right)$$

$$\tau_{xy} = \tau_{yx} = \mu\left(\frac{\partial u}{\partial y} + \frac{\partial v}{\partial x}\right)$$

and

$$\tau_{yy} = \frac{2}{3}\mu\left(2\frac{\partial v}{\partial y} - \frac{\partial u}{\partial x}\right)$$

and assumptions $E_x = E_y = B_x = B_z = 0$ are used to obtain the preceding simplified equations. E_z is generally not zero, and B_x is the induced magnetic field in which variable $|B_x| \ll |B_0|$. The low-magnetic-Reynolds-number assumption renders the preceding simplified equations variable. Otherwise, a full group of MGD equations, including one continuity equation, three momentum equations, one energy equation, one equation of state, and three magnetic field equations must be used [30,33].

In this study, we consider the velocity-slip and temperature-jump wall boundary conditions [34]:

$$u_w(x, y) = \frac{2 - \sigma_u}{\sigma_u}\lambda(x, y)\left(\frac{du}{dn}\right)_w + \frac{3}{4}\frac{\mu}{\rho T_w}\left(\frac{\partial T}{\partial x}\right)_w, \qquad y = \pm d \tag{6}$$

$$T_w(x, y) = \frac{2 - \sigma_T}{\sigma_T}\frac{2\gamma}{Pr(\gamma + 1)}\lambda(x, y)\left(\frac{dT}{dn}\right)_w, \qquad y = \pm d \tag{7}$$

where $\lambda = 1/(\sqrt{2}\pi D^2 n(x, y))$ is the local molecule mean free path; D and n are the atomic diameter and number density, respectively; σ_u is the momentum accommodation coefficient; σ_T is the energy accommodation coefficient; and Pr is the Prandtl number.

III. Order Estimations

As we will see in the next section, a proper order estimation for several nondimensional parameters is crucial to simplify the governing equations. Hence, before we proceed to simplify the equations, we need to first estimate the orders of magnitude for several nondimensional parameters, including Mach number $Ma = U_o/\sqrt{\gamma RT_o}$, Reynolds number $Re = (2d)\rho_o U_o/\mu$, magnetic force number $R_b = B_0^2/(\rho_o U_o^2 \mu_m)$, magnetic Reynolds number $Re_\sigma = (2d)U_o\mu_o\sigma_o$, Knudsen number

$$Kn = \frac{\lambda}{2d} \sim \sqrt{\frac{\pi\gamma}{2}}\frac{Ma}{Re}$$

and Hartmann number $Ha = \sqrt{ReR_\sigma R_b}$. These nondimensional numbers are based on the quantities at the outlet and the external magnetic field.

Similar to our previous study [20], by choosing the whole flow domain as an integral domain and exercising the X momentum equation globally, we obtain

$$\begin{aligned}&2d(P_o - P_i + \rho_o U_o^2 - \rho_i U_i^2) \\ &\quad = \mu\frac{U_i + U_o}{2d}2L - \sigma B_0\left(E_z + \frac{U_o + U_i}{2}B_0\right)2dL\end{aligned}$$

Further, because the average inlet speed U_i is generally much smaller than the average outlet speed U_o for a pressure-driven gas flow inside a microchannel, those terms with U_i are dropped. Then the following simple relation can be obtained:

$$\epsilon(1 + 1/(\gamma Ma^2)(1 - 1/P)) \sim 1/Re + R_\sigma R_b \tag{8}$$

where $P = p_i/p_o$ and $\epsilon = 2d/L$. The parameter K, which is a key physical factor for the microchannel flow, presenting the ratio between the electric field to the magnetic field. Here, it is considered to be the same order or less than the magnetic field effects, and it is combined into the factor $R_\sigma R_b$.

This simple relation [Eq. (8)] contains four nontrivial terms:

1) The momentum change term is represented by ϵ on the left-hand side.

2) The pressure drop term applying at the channel inlet and outlet is $\epsilon/(\gamma Ma^2)(1 - 1/P)$ on the left-hand side.

3) The viscous force along the wall surfaces is $1/Re$ on the right-hand side.

4) The magnetic/electric force applies to the whole domain $R_\sigma R_b$ on the right-hand side.

There are many choices to balance these terms: all terms can share the same order of magnitudes; three terms share the same larger order, whereas the other term is smaller; two of the four terms are larger, whereas the other two terms are equally smaller; or two of the four terms are large, one term is relatively small, and the other term is the smallest. Hence, from the preceding four permutations, there will be at least

$$1 + C_4^3 + C_4^2 C_2^2 + C_4^2 C_2^1 = 23$$

classes of combinations, and most of these combinations can have many detailed subclasses as well. Here, we are interested in investigating the interactions among viscous stress, pressure drop, and magnetic/electric field effects. Different parameter orders may

result in different simplified governing equations and different flow solutions, including hypersonic, supersonic, and transonic flows, as we illustrated in our previous paper [20].

Of the numerous possible parameter combinations, in this study, we are specially interested in slow MGD flows under the effects of strong pressure difference, strong viscous effects along the channel wall, and strong MGD force. It is well known that the external magnetic and electric fields change the velocity profile inside the channel and that there is a thin Hartmann layer next to the wall. We assume that the momentum gain term at the outlet is relatively small when compared with the other three terms. This assumption is reasonable, because in the limiting case of an exact Hartmann flow, the velocity profile remains unchanged and the momentum change term is zero. In this study, we select two viable cases with the following parameter combinations, which satisfy Eq. (8):

1) Case 1 is $Re \sim \epsilon$, $Ma \sim \epsilon$, $Kn \sim 1$, $R_b \sim 1/\epsilon^2$, $R_\sigma \sim \epsilon$, and $H_a \sim 1$.

2) Case 2 is $Re \sim 1$, $Ma \sim \epsilon^{1/2}$, $Kn \sim \epsilon^{1/2}$, $R_b \sim 1/\epsilon$, $R_\sigma \sim \epsilon$, and $H_a \sim 1$.

In our previous study [20], we showed that the Reynolds and Mach numbers in these two cases render a balance between the viscous effects and the pressure drop term. We intend to set R_σ at least one order smaller than R_b to create a very small induced magnetic field, but the magnetic interaction factor $Q = R_\sigma R_b$ is assumed to be as strong as the terms for viscous force and pressure drop.

IV. Asymptotic Solutions

In this study, the flow quantities are normalized with the averaged properties at the outlet, and the X and Y coordinates are normalized with L and $2d$, respectively [5,20]. For the rest of the paper, it is assumed that the coordinates and properties are nondimensional, unless we clearly state otherwise.

With the two sets of parameters previously selected, the nondimensional normalized governing equations and boundary conditions are

$$\epsilon\frac{\partial(\rho u)}{\partial x}+\frac{\partial(\rho v)}{\partial y}=0 \tag{9}$$

$$\epsilon\frac{\partial}{\partial x}\left(\rho uu+\frac{p}{\gamma M_a^2}\right)+\frac{\partial(\rho vu)}{\partial y} =\frac{1}{Re}\left(\epsilon^2\frac{4}{3}\frac{\partial^2 u}{\partial x^2}+\frac{\partial^2 u}{\partial y^2}+\frac{1}{3}\epsilon\frac{\partial^2 v}{\partial x\partial y}\right)+Q(K-u) \tag{10}$$

$$\epsilon\frac{\partial(\rho uv)}{\partial x}+\frac{\partial}{\partial y}\left(\rho v^2+\frac{p}{\gamma M_a^2}\right)=\frac{1}{Re}\left(\epsilon^2\frac{\partial^2 v}{\partial x^2}+\frac{4}{3}\frac{\partial^2 v}{\partial y^2}+\epsilon\frac{\partial^2 u}{\partial x\partial y}\right) \tag{11}$$

$$\begin{aligned}\epsilon\rho u\frac{\partial T}{\partial x}+\rho v\frac{\partial T}{\partial y}&=\epsilon\frac{\gamma-1}{\gamma}u\frac{\partial p}{\partial x}+\frac{\gamma-1}{\gamma}v\frac{\partial p}{\partial y}\\&+\frac{1}{RePr}\left(\epsilon^2\frac{\partial^2 T}{\partial x^2}+\frac{\partial^2 T}{\partial y^2}\right)+\frac{(\gamma-1)M^2}{Re}\\&\times\left[2\left(\frac{\partial u}{\partial x}\right)^2\epsilon^2+2\left(\frac{\partial v}{\partial y}\right)^2+\left(\epsilon\frac{\partial v}{\partial x}+\frac{\partial u}{\partial y}\right)^2\right.\\&\left.-\frac{2}{3}\left(\frac{\partial u}{\partial x}\epsilon+\frac{\partial v}{\partial y}\right)^2\right]+QK(K-u)\end{aligned} \tag{12}$$

$$p=\rho T=nT \tag{13}$$

$$u_1(x,y)|_{y=\pm 1/2}=\Theta_u Kn(x)|_{y=\pm 1/2}\left.\frac{\partial u_1(x,y)}{\partial n}\right|_{y=\pm 1/2} \tag{14}$$

$$T|_{y=\pm 1/2}-T_w=\Theta_T\frac{2\gamma}{Pr(\gamma+1)}Kn(x)\left(\frac{\partial T}{\partial n}\right)_{y=\pm 1/2} \tag{15}$$

where the relations $|v|<|u|$ and $|B_x|\ll|B_0|$ are used to simplify the source terms in the momentum and energy equations $\Theta_u=(2-\sigma_u)/\sigma_u$ and $\Theta_T=(2-\sigma_T)/\sigma_T$. In Eq. (14) for the nondimensional velocity boundary condition, the temperature gradient term is omitted because it is relatively smaller than the velocity gradient term for the two specific groups of nondimensional parameters.

Further, we assume the following series expansions:

$$u=u_1+\epsilon u_2+\quad\cdots\quad v=v_1+\epsilon v_2+\quad\cdots\quad p=p_1+\epsilon p_2+\quad\cdots$$

$$\rho=\rho_1+\epsilon\rho_2+\quad\cdots\quad n=n_1+\epsilon n_2+\quad\cdots\quad T=1+\epsilon T_2+\quad\cdots$$

The last expression implies a quasi-isothermal assumption [20], which is based on the fact that if the flow speed inside the microchannel is not large, then the temperature variations should be small. This assumption leads to the temperature-field solution. Especially, from

$$p(x,y)=\rho(x,y)(1+\epsilon T_2(x,y))$$

we obtain $p_1=\rho_1$ as the zero-order relation, and the isothermal assumption proposed by Arkilic et al. [5] is relaxed.

For the two sets of parameters, the Y momentum equation simplifies with the only leading term:

$$\frac{\partial p_1(x,y)}{\partial y}=0 \tag{16}$$

With the low-magnetic-Reynolds-number assumption, the corresponding magnetic term is at least one order smaller than the pressure term. It is obvious from Eq. (16) that $p_1(x,y)=p_1(x)$, which greatly simplifies the following derivations.

The simplified X momentum equation is the same as that for the Hartmann flow [29]:

$$\frac{\partial^2 u_1}{\partial y^2}-Ha^2u_1=-Ha^2K+\frac{\epsilon Re}{\gamma Ma^2}\frac{dp_1}{dx} \tag{17}$$

But the velocity-slip wall boundary conditions result in different solutions from the classical Hartmann flow solutions with nonslip wall boundary conditions. The final U velocity solution is

$$u_1(x,y)=C_1\frac{\epsilon Re}{\gamma M^2}\frac{dp_1}{dx}\cosh(Hay)-\frac{\epsilon Re}{Ha^2\gamma M^2}\frac{dp_1}{dx}+K \tag{18}$$

where

$$C_1=\frac{1}{Ha^2C_2}-\frac{K\gamma M^2}{C_2\epsilon Re(dp_1/dx)}$$

$$C_2=\cosh\left(\frac{Ha}{2}\right)+\Theta_u Kn(x)\sinh\left(\frac{Ha}{2}\right)Ha$$

Note that Eqs. (17) and (18) are of order one, because the flow parameters chosen will render these terms to become the same order as the rest in these equations.

The zero-order solution for the V velocity is obtained from the zero order of the continuity equation $v_1=0$, and the next order can be obtained from the continuity equation by using the relation $\rho_1=p_1$:

$$\frac{\partial(p_1(x)u_1(x,y))}{\partial x}+\frac{\partial(p_1(x)v_2(x,y))}{\partial y}=0$$

The result is

$$\begin{aligned}v_2(x,y)&=A_1\sinh(Hay)\left[-\frac{1}{2}\frac{d^2p_1^2}{p_1dx^2}+A_2\frac{d^2p_1}{p_1dx^2}\right]\\&+A_3K\frac{dp_1}{p_1dx}\sinh(Hay)+y\frac{\epsilon Re}{2Ha^2\gamma M^2}\frac{d^2p^2}{p_1dx^2}-\frac{dp_1}{p_1dx}Ky\end{aligned} \tag{19}$$

where

$$A_1 = \frac{\epsilon Re}{\gamma M^2 Ha^3 \cosh(Ha/2)}$$

$$A_2 = \Theta_u Ha Kn_o \tanh(Ha/2)$$

$$A_3 = \frac{1}{Ha \cosh(Ha/2)}$$

The temperature distribution can be obtained by the following simplified energy equation and the temperature-jump wall boundary conditions:

$$\frac{1}{RePr}\frac{\partial^2 T_2}{\partial y^2} = -\frac{\gamma-1}{\gamma}u_1\frac{dp_1}{dx} - \frac{(\gamma-1)M^2}{\epsilon Re}\left(\frac{\partial u_1(x,y)}{\partial y}\right)^2 - QK(K-U) \tag{20}$$

The solution for the temperature field is

$$T_2(x,y) = RePr\left(\frac{N_3}{Ha^2}\cosh(Hay) + \frac{N_5}{4Ha^2}\cosh(2Hay) + \frac{N_6}{2}y^2 + N_8\right) \tag{21}$$

where N_8 is determined by the temperature-jump boundary condition:

$$N_8 = \frac{T_w - 1}{\epsilon RePr} - \frac{N_3}{Ha^2}\cosh\left(\frac{Ha}{2}\right) - \frac{N_5}{4Ha^2}\cosh(Ha) - \frac{N_6}{8} - \Theta_T\frac{2\gamma Kn(x)}{Pr(\gamma+1)}\left[\frac{N_3}{Ha}\sinh\left(\frac{H_a}{2}\right) + \frac{N_5}{2Ha}\sinh(Ha) + \frac{N_6}{2}\right]$$

Moreover,

$$N_1 = C_1\frac{\epsilon Re}{\gamma M^2}\frac{dp_1}{dx}$$

$$N_2 = -\frac{\epsilon Re}{H_a^2\gamma M^2}\frac{dp_1}{dx} + K$$

$$N_3 = -\frac{\gamma-1}{\gamma}N_1\frac{dp_1}{dx} + QKN_1$$

$$N_4 = -\frac{\gamma-1}{\gamma}N_2\frac{dp_1}{dx} - QK^2 + QKN_2$$

$$N_5 = -\frac{(\gamma-1)M^2}{2\epsilon Re}N_1^2 Ha^2$$

and $N_6 = N_4$–N_5. The density distribution is approximated as

$$\rho(x,y) = p_1(x)/(1 + \epsilon T_2(x,y)$$

It is evident that the density is not constant at any specific station with $x =$ constant.

The pressure distribution is crucial to the whole set of the solution, because $p(x)$ and its gradients dominate the coefficients for $u(x,y)$, $v(x,y)$, and $T(x,y)$. Evaluating the V velocity along the upper channel wall results in the following equation:

$$D_1\frac{d^2p_1^2}{dx^2} + D_2\frac{d^2p_1}{dx^2} + D_3K\frac{dp_1}{dx} = 0 \tag{22}$$

where

$$D_1 = -\left(\frac{\tanh(Ha/2)}{2Ha^3} - \frac{1}{4Ha^2}\right)\frac{\epsilon Re}{\gamma M^2}$$

$$D_2 = \frac{\tanh^2(Ha/2)}{Ha^2}\frac{\epsilon Re}{\gamma M^2}\Theta_u Kn_o$$

and

$$D_3 = -\frac{1}{2} + \frac{\tanh(Ha/2)}{Ha}$$

With the boundary conditions $p_1(0) = P$ and $p_1(1) = 1$, the following exact solutions to the nonlinear ordinary differential equation are obtained:

1) If $K = 0$ (i.e., in the absence of the electric field effect),

$$p_1(x) = \frac{-D_2 + \sqrt{D_2^2 + 4D_1(D_1P^2 + D_2P + D_4x)}}{2D_1} \tag{23}$$

where $D_4 = D_1(1-P^2) + D_2(1-P)$.

2) If $K > 0$ (i.e., with a uniform electric field),

$$2D_1p_1(x) + \left(\frac{2D_1G_1}{D_3K} + D_2\right)\ell n[D_3Kp_1(x) - G_1] = -xD_3K + G_2D_3K \tag{24}$$

The two boundary conditions exactly determine the coefficients G_1 and G_2 in the preceding solution:

$$G_2 = \frac{2D_1}{D_3K} + \left(\frac{2D_1G_1}{D_3^2K^2} + \frac{D_2}{D_3K}\right)\ell n(D_3K - G_1) + 1$$

and

$$2D_1(P-1) - D_3K = \left(\frac{2D_1G_1}{D_3K} + D_2\right)\ell n\left(\frac{D_3K - G_1}{D_3KP - G_1}\right)$$

Solving for G_1 requires an iterative method. However, for a given set of nondimensional numbers, G_1 and G_2 are completely determined.

The nondimensional mass flow rate through the channel is

$$Q(x,y) = \int_{-1/2}^{1/2}\rho(1,y)u_1(1,y)\mathrm{d}y = \left(\frac{2}{Ha^3}\tanh\frac{Ha}{2}\left(1 - \Theta_u Kn_o Ha\tanh\frac{Ha}{2}\right)\frac{\epsilon Re}{\gamma M^2}F - \frac{2K}{Ha}\tanh\frac{Ha}{2}\left(1 - \Theta_u Kn_o Ha\tanh\frac{Ha}{2}\right) + K - \frac{\epsilon Re}{Ha^2\gamma M^2}F\right) \tag{25}$$

where

$$F = \frac{dp(x)}{dx}|_{x=1}$$

A more detailed format can be obtained with the known exact pressure solutions.

Some remarks to conclude this section are as follows:

1) Our derivation is based on two specific sets of nondimensional parameters; in particular, the convection term is omitted. Here, careful treatment of the parameters is essential. For example, it is straightforward to see from Eq. (17) that if the Hartmann number is large, then the U-velocity profile is straight, except inside the Hartmann layer. However, a large Hartmann number with a nonzero electric field can lead to large temperature changes; hence, it would

defy the quasi-isothermal assumption, which is crucial to obtain the pressure solutions.

2) Note that many other possible asymptotic solutions with different combinations of nondimensional parameters exist; some cases can even be supersonic and hypersonic [20]. With an isothermal assumption, the results are only applicable to long microchannels or channels; with the quasi-isothermal assumption, the results can apply to a wider range of microchannels or channels of conventional dimensions. The Joule heating effects can be included, as long as the temperature change is of the order of ϵ.

3) We want show that our microchannel MGD solutions are related to that of the classical Hartmann flow as a specific case. To do so, we will use the nonslip and constant-temperature wall boundary condition instead of the boundary conditions here [Eqs. (14) and (15)], whereas taking the limit of ϵ goes to zero.

a) For the pressure distribution, $D_2 = 0$ in Eq. (22) with the vanishing ϵ limit whereby the two solutions for the pressure distribution merge into a general solution:

$$p_1(x) = \frac{-D_3K + \sqrt{D_3^2K^2 + 4D_1(D_1P^2 + D_3KP + D_5x)}}{2D_1} \tag{26}$$

where

$$D_5 = D_1(1 - P^2) + D_3K(1 - P)$$

Thus, Eq. (26) becomes

$$p(x) = -Q_0 + \sqrt{Q_1 - Q_2x}$$

with $Q_1 > Q_2 > 0$. Because $0 < x < 1$, after expanding the term inside the square root and neglecting the higher orders of x, a linear pressure distribution for the classical Hartmann flow is recovered. However, to accurately compute for the flow inside a channel of finite length, higher-order terms for pressure gradients must be considered.

b) For U velocity, $C_2 = \cosh(Ha/2)$ in Eq. (18), in which C_1 remains the same. If the higher order of pressure gradient terms is neglected, with the linear pressure gradient as the classical Hartmann flow, then the classical Hartmann flow with a constant-velocity profile at each station is recovered. For microchannel flows, the nonconstant-velocity profiles are created by two factors: the velocity-slip wall boundary condition with the $Kn(x)$ factor and the nonlinear pressure gradient term.

c) For V velocity, A_1 and A_3 remain the same, but $A_2 = 0$ in Eq. (19).

d) For the temperature field,

$$N_8 = \frac{T_w - 1}{\epsilon RePr} - \frac{N_3}{Ha^2}\cosh\frac{Ha}{2} - \frac{N_5}{4Ha^2}\cosh Ha - \frac{N_6}{8}$$

in Eq. (21), in which other constants remain the same.

V. Numerical Validations

To validate the preceding analytical results, we perform numerical computations to solve the low-magnetic-Reynolds-number MGD equations, and we compare the results with the corresponding analytical results. The computations are performed with a well-tested general Navier–Stokes equation solver; specifically, we apply this Navier–Stokes equation solver to the formulation of Eqs. (1–7). The Navier–Stokes equation solver uses the classical Roe scheme to compute inviscid fluxes and a central difference scheme to compute viscous fluxes. The solver adopts the minmod function to reconstruct the gradient properties. The flow parameters are $\epsilon = 0.06$, $L = 20\ \mu$m, $p_1 = 2$ atm, $p_2 = 1$ atm, $T_1 = 300$ K, $\sigma_u = \sigma_T = 0.85$, oxygen gas, $\gamma = 1.4$, $Pr = 0.72$, $\mu = 1.919 \times 10^{-5}$ s $\cdot$ N/m^2, wall temperature $T_w = 300$ K, $R_b = 1/\epsilon$, and $R_\sigma = \epsilon$. When the magnetic field is enabled, K is chosen to be 0.0, 0.5, or 0.9. Many of these simulation parameters are the same as those in our previous paper [20] on a neutral-gas-flow case.

The first set of results, Figs. 2–6, correspond to a case with $K = 0.5$, the so-called impedance match case for Hartmann flow [32]. This set of results contains both electric and magnetic field effects. We use this case to validate the general solutions for the flow and temperature fields.

Figure 2 shows the pressure contours, and the contours are generally straight and the comparisons are good. Figures 3 and 4 show comparisons of U- and V-velocity results, in which in the former the velocity-slip effects are very evident along the wall and the latter shows some discrepancies at the outlet boundary. Overall, the velocity field solutions agree well. Figure 5 shows the density contours, which are slightly curved. The analytical results are obtained from

$$\rho(x, y) = p(x)/(1 + \epsilon T_2(x, y))$$

The quasi-isothermal assumption permits curved analytical density contours, as expected. The numerical-vs-analytical discrepancy is caused by the error from pressure and temperature passing to the density results. Figure 6 shows comparisons of numerical and analytical temperature results. In general, the temperature fields have the same trends, but discrepancies are found to be larger than with the U- and V- velocity fields. Some explanations accounting for the discrepancies will be discussed later.

The second set of comparisons presented in Figs. 7–12 is based on four different cases: 1) no magnetic and electric fields, 2) magnetic field only with $K = 0$, 3) magnetic and electric fields with $K = 0.5$, and 4) magnetic and electric fields with $K = 0.9$. We intend to show some trends by comparing the results from these four cases. The first

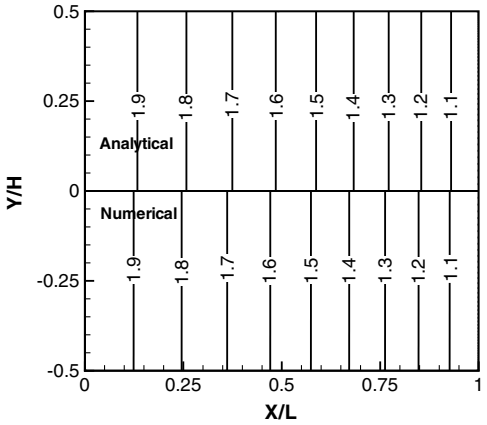

Fig. 2 Comparison of pressure contours, $P = 2$, $K = 0.5$, $R_b = 1/\epsilon$, $R_\sigma = \epsilon$, and $\epsilon = 0.06$.

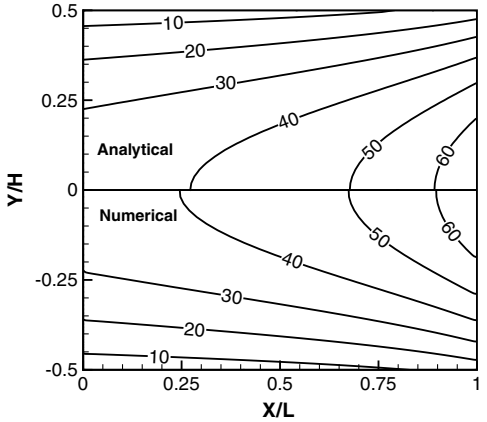

Fig. 3 Contours of U velocity, $P = 2$, $K = 0.5$, $R_b = 1/\epsilon$, $R_\sigma = \epsilon$, and $\epsilon = 0.06$.

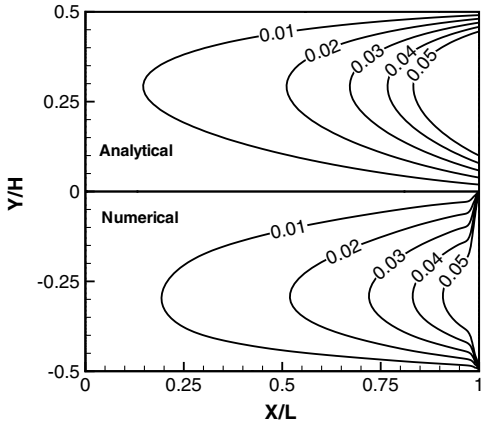

Fig. 4 Contours of V velocity, $P = 2$, $K = 0.5$, $R_b = 1/\epsilon$, $R_\sigma = \epsilon$, and $\epsilon = 0.06$.

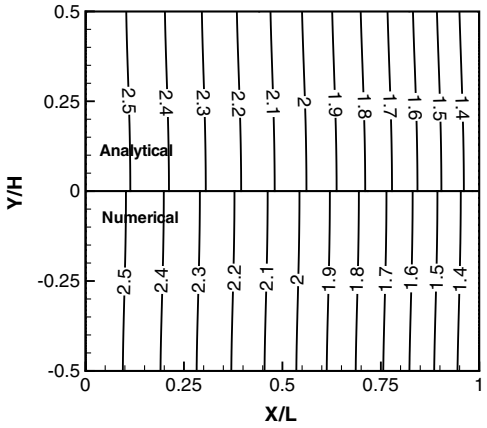

Fig. 5 Contours of density, $P = 2$, $K = 0.5$, $R_b = 1/\epsilon$, $R_\sigma = \epsilon$, and $\epsilon = 0.06$.

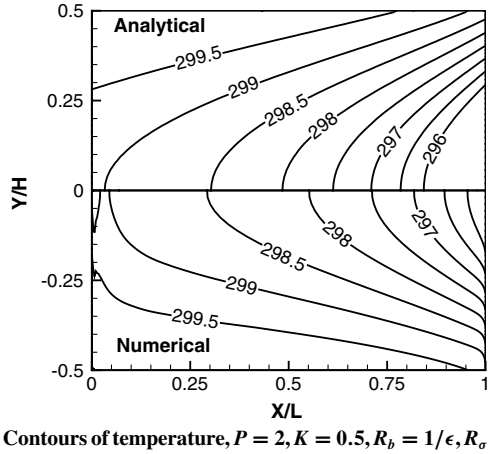

Fig. 6 Contours of temperature, $P = 2, K = 0.5, R_b = 1/\epsilon, R_\sigma = \epsilon$, and $\epsilon = 0.06$.

case is governed by the classical Navier–Stokes equations, and there are previous analytical solutions available [5,20]. The second case contains an extra term contributed by the magnetic field to the X momentum equation, but not to the energy equation. The third case contains both electric and magnetic fields. The last case contains stronger electric and magnetic field effects. The electric and magnetic fields have strong impacts on the temperature results. For each case, the electric field is constant through the whole flowfield. The magnetic field effects are not constant with uB_0 in the source terms, because B_0 is constant, but u_1 is not uniform throughout the field. Hence, the nonuniform strength of sources terms is added to the X momentum and the energy equations for the last two cases. Thus, four sets of combinations can offer some physical insights into the different contributions from the magnetic and electric fields.

Figure 7 shows the pressure distributions along the flow direction, with the linear pressure distributions subtracted. The lines without solid symbols are analytical results, whereas the line with solid symbols represents the numerical simulation results for the last case. Numerical solutions are obtained for all cases; here, we merely present one case of $K = 0.9$, for clarity. It is clear that the linear pressure gradient assumed in the Hartmann flow is not applicable here and it may result in inaccuracies if used carelessly. For these four test cases, at any specific station, pressure level increases from case 1 to case 4, indicating that the extra magnetic field or electric field results in increasingly stronger impedance to the flowfield. For cases 3 and 4, the numerical and analytical results are essentially the same, whereas for the last two cases, the nonlinearities become more appreciable. Larger discrepancies are found for cases 3 and 4 between numerical simulations and analytical results than for cases 1 and 2.

Figure 8 shows the different U-velocity profiles for the four test cases at the middle station of the channel, $x/L = 0.5$. It shows that the electric and magnetic fields have a strong influence on the velocity profiles. Figure 9 shows the different V-velocity profiles for the four test cases at the middle section of the channel. It is very obvious that the V velocities are much smaller than the U velocities. Only the upper half of results with a positive V velocity are presented, for a better illustration; the other half of the results have negative values and are antisymmetric to the upper part. Again, for all the cases, the numerical and analytical results are close. For clarity, only

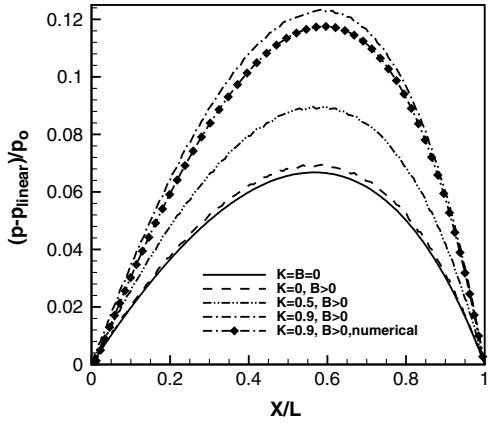

Fig. 7 Pressure distribution along the flow direction, $P = 2$, $R_b = 1/\epsilon$, $R_\sigma = \epsilon$, and $\epsilon = 0.06$.

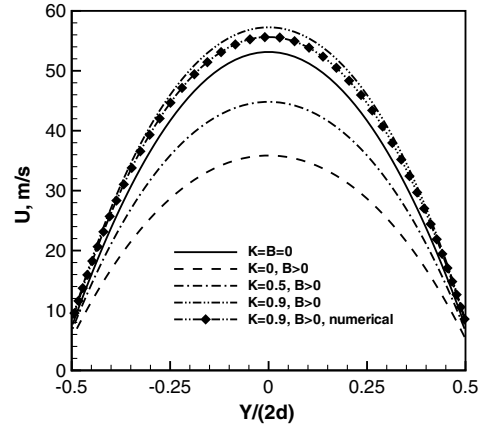

Fig. 8 Profiles of U velocity distributions at the middle section, $x/L = 0.5$, $P = 2$, $R_b = 1/\epsilon$, $R_\sigma = \epsilon$, and $\epsilon = 0.06$.

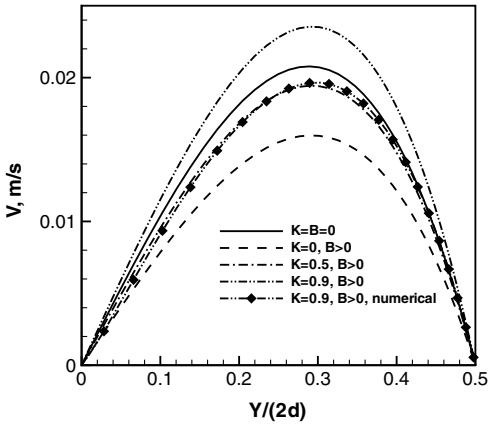

Fig. 9 Profiles of V velocity at the middle section, $x/L = 0.5$, $y > 0$, $P = 2$, $R_b = 1/\epsilon$, $R_\sigma = \epsilon$, and $\epsilon = 0.06$.

the numerical results of case 4 are shown. Figure 10 shows the profiles of velocity slips along the upper walls for these four test cases. In general, the slip velocities increase as gas flows downstream, and the numerical results are found to agree with the analytical results. Essentially, for the last two cases, the gas flows are both Fanno and Rayleigh flows, due to the wall friction and Joule heating effects. Hence, with stronger Joule heating effects in case 4, the subsonic flow increases its speed more significantly toward the sonic speed than that of case 3 [35].

Now some words are in order concerning the discrepancies found on the results:

1) The numerical simulation results are from the whole MGD equations, whereas the analytical solutions are based on the asymptotic equations. If we consider the truncation error $\mathcal{O}(\epsilon)$ as an upper limit, then there is about a 6% theoretical difference with $\epsilon = 0.06$.

2) The analytical results are actually based on the assumption that the channel is in the middle of the flowfield without entrance effects; however, for numerical solutions, the entrance effects are not avoidable, due to the presence of significant friction occurring at the inlet region. The uniform freestream needs to adjust to the channel flow around the inlet entrance. The inlet and outlet boundary condition treatments are very subtle, and the outlet boundary condition treatment is also important because the gradients there are large. However, these end boundary effects are not included in the asymptotic solutions at all. Significant discrepancies therefore show up in the V velocity and temperature profiles.

3) Between the analytical and numerical solutions, the pressure fields already have some discrepancies, and with the small length dimension, dp/dx and dp^2/dx^2 must be huge quantities. For the temperature field, the dp/dx term dominates in the coefficients, and $(dp/dx)^2$ appears in the coefficients N_5 and N_6. Hence, it is not surprising to see that the temperature profiles have poorer agreement than the velocity and pressure results.

4) Analytically, we only consider the leading term for the electric and magnetic field effects, and because they are coupled in the source terms for the momentum and energy equations, some nonlinear effects are possible.

Finally, Figs. 11 and 12 show the temperature profiles and the temperature gradients along the upper wall boundary. As discussed earlier, it is very difficult to obtain accurate temperature profiles, especially when both electric and magnetic fields are considered. Hence, these plots only show the analytical results. For cases $K = 0.5$ and 0.9, there are Joule heating effects in the energy equation. For $K = 0.9$, stronger Joule heating deposits more energy into the field, resulting in a much higher increase in the averaged temperature. As shown in Fig. 11, a portion of gas close to the wall is actually hotter than the wall. Correspondingly, for the last case, heat flux is transferred into the wall instead from the wall, as shown by Fig. 12. There, it also indicates one important effect associated with an MGD gas flow inside a microchannel: along the wall, even when the temperature change is very small, the normal temperature gradient can be huge because of the narrow-channel height [20]. Hence, this shows that the heat transfer problem in microchannels is of practical importance. For case 1 ($K = 0$) without any electric and magnetic field effects, the temperature gradient reaches an order of 1×10^6 K/m. By contrast, with magnetic and electric field effects ($K = 0.9$), the magnitude of temperature gradient becomes much larger and variant, as shown in Fig. 12.

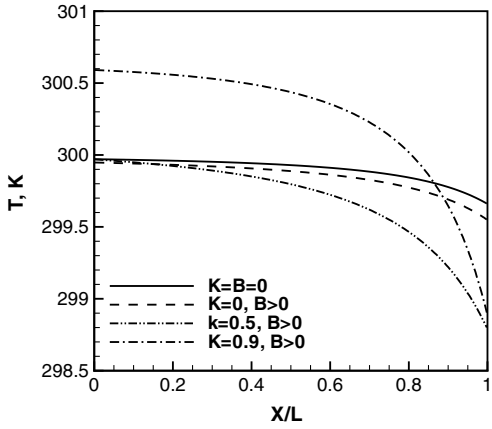

Fig. 11 Profiles of temperature distributions along the upper wall, $P = 2$, $R_b = 1/\epsilon$, $R_\sigma = \epsilon$, and $\epsilon = 0.06$.

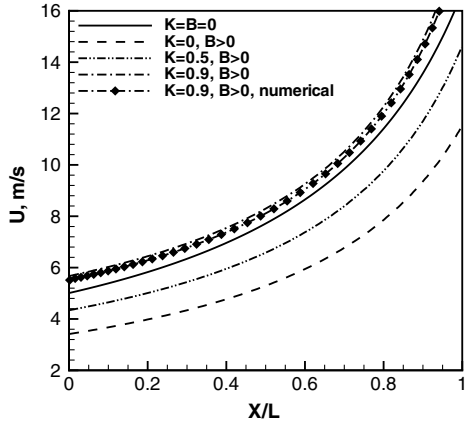

Fig. 10 Profiles of slip velocity along the wall, $y = d$, $P = 2$, $R_b = 1/\epsilon$, $R_\sigma = \epsilon$, and $\epsilon = 0.06$.

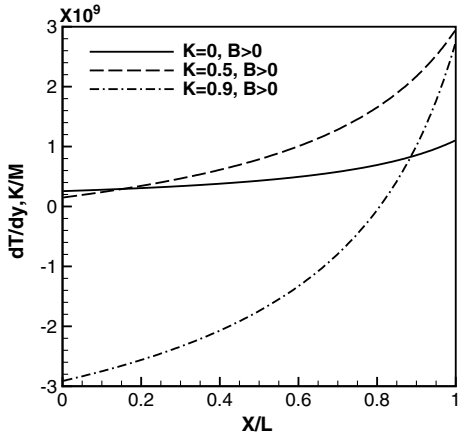

Fig. 12 Profiles of temperature gradient along the upper wall, $P = 2$, $R_b = 1/\epsilon$, $R_\sigma = \epsilon$, and $\epsilon = 0.06$.

VI. Conclusions

We have reported an analysis of rarefied MGD gas flows inside a two-dimensional microchannel with velocity-slip and temperature-jump boundary conditions and with the assumptions that the magnetic Reynolds number is low and the flow is quasi-isothermal. By carefully comparing different orders of magnitude for the pressure drop, viscous shear stress at the channel wall, and the magnetic forces, two sets of parameters are selected and used to simplify the MGD equations. This study yields asymptotic solutions for velocity components, pressure, and temperature, which revert to the Hartmann flow solution under specific conditions. With stronger Joule heating effects, the Rayleigh effects become significant, and the average pressure, velocity, and temperature inside the channel increase. In general, the pressure gradient along the flow direction is nonlinear inside the channel, and the velocity and density distributions are nonuniform. Numerical solutions of the same formulation are obtained to validate these asymptotic solutions; explanations are provided for the discrepancies found between these two solutions.

Acknowledgments

Most of the work was accomplished when Chunpei Cai worked as a computational fluid dynamics specialist for ZONA Technology. It was partially supported by the ZONA Internal Research and Development Funding. The authors would like to thank one reviewer and Banavara Shashikanth for valuable suggestions and helpful comments, leading to the present version. Cai would also like to thank Iain D. Boyd for an earlier discussion about the treatments of parameter estimations, quasi-isothermal assumption, and temperature solution. These treatments are crucial for the work in our previous paper [20] and eventually led to the work in this paper.

References

[1] Prud'homme, R. K., Chapman, T. W., and Brown, J. R., "Laminar Compressible Flow in a Tube," *Applied Scientific Research*, Vol. 43, Mar. 1986, pp. 67–74. doi:10.1007/BF00385729

[2] Van Den Berg, H. R., Seldam, C. A., and Van der Guli, P. S., "Compressible Laminar Flow in a Capillary," *Journal of Fluid Mechanics*, Vol. 246, Jan. 1993, pp. 1–20. doi:10.1017/S0022112093000011

[3] Harley, J. C., and Huang, Y. H., "Gas Flow in Micro-Channels," *Journal of Fluid Mechanics*, Vol. 284, 1995, pp. 257–274. doi:10.1017/S0022112095000358

[4] Ho, C.-M., and Tai, Y.-C., "Micro-Electro-Mechanical-Systems (MEMS) and Fluid Flows," *Annual Review of Fluid Mechanics*, Vol. 20, Jan. 1998, pp. 579–612. doi:10.1146/annurev.fluid.30.1.579

[5] Arkilic, E. B., Schmidt, M. A., and Breuer, K. S., "Gaseous Slip Flow in Long Microchannels," *Journal of Microelectromechanical Systems*, Vol. 6, No. 2, June 1997, pp. 167–178. doi:10.1109/84.585795

[6] Karniadakis, G. E., and Beskok, A., *Microflows: Fundamentals and Simulation*, Springer, New York, 2002.

[7] Zohar, Y., Lee, S. Y. K. Lee, W. Y., Jiang, L., and Tong, P., "Subsonic Gas Flow in a Straight and Uniform Microchannel," *Journal of Fluid Mechanics*, Vol. 472, Dec. 2002, pp. 125–151.

[8] Ho, C. M., and Tai, Y. C., "Micro-Electro-Mechanical Systems (MEMS) and Fluid Flows," *Annual Review of Fluid Mechanics*, Vol. 30, 1998, pp. 579–612. doi:10.1146/annurev.fluid.30.1.579

[9] Zheng, Y., Garcia, A. L., and Alder, B. J., "Comparison of Kinetic Theory and Hydrodynamics for Poiseuille Flow," *Journal of Statistical Physics*, Vol. 109, Nos. 3–4, Nov. 2002, pp. 495–505. doi:10.1023/A:1020498111819

[10] Oran, E. S., Oh, C. K., and Cybyk, B. Z., "Direct Simulation Monte Carlo: Recent Advances and Applications," *Annual Review of Fluid Mechanics*, Vol. 30, pp. 403–441. doi:10.1146/annurev.fluid.30.1.403

[11] Cai, C., Boyd, I., Fan, J., and Candler, G. V., "Direct Simulation Methods for Low-Speed Microchannel Flows," *Journal of Thermophysics and Heat Transfer*, Vol. 14, July–Sept. 2000, pp. 368–378. doi:10.2514/2.6534

[12] Fan, J., and Shen, C., "Statistical Simulation of Low-Speed Unidirectional Flows in Transition Regime," *21st International Symposium on Rarefied Gas Dynamics*, Vol. 2, Cepadus-Editions, Toulouse, France, 1998, pp. 245–252.

[13] Aristov, V. V., *Direct Methods for Solving the Boltzmann Equations and Study of Nonequilibrium Flows*, Kluwer, Dordrecht, The Netherlands, 2001.

[14] Ohwada, T., Sone, Y., and Aoki, K., "Numerical Analysis of the Poiseuille Flow and Thermal Transpiration Flows Between Two Parallel Plates on the Basis of the Linearized Boltzmann Equation for Hard-Sphere Molecules," *Physics of Fluids*, Vol. 1, No. 12, 1989, pp. 2042. doi:10.1063/1.857478

[15] Xu, K., and Li, Z., "Microchannel Flow in the Slip Regime: Gas-Kinetic BGK-Burnett Solutions," *Journal of Fluid Mechanics*, Vol. 513, No. 513, Aug. 2004, pp. 87–110. doi:10.1017/S0022112004009826

[16] Chen, C. K., and Weng, H. C., "Developing Natural Convection with Thermal Creep in a Vertical Microchannel," *Journal of Physics D: Applied Physics*, Vol. 39, No. 14, July 2006, pp. 3107–3118. doi:10.1088/0022-3727/39/14/034

[17] Du, D. X., Li, Z. X., and Guo, Z. Y., "Effect of Reversible Work and Viscous Dissipation on Gas Flow Characteristics in a Microtube," *Journal of Tshinghua University. Science and Technology*, Vol. 39, No. 11, 1999, pp. 89–94.

[18] Qin, F. H., Sun, D. J., and Yin, X. Y., "Perturbation Analysis Gas Flow in a Straight Microchannel," *Physics of Fluids*, 19, 2007, Paper 027103. doi:10.1063/1.2564671

[19] Wang, M., and Li, Z., "Micro- and Nanoscale Nonideal Gas Poiseuille Flows in a Consistent Boltzmann Algorithm Model," *Journal of Micromechanics and Microengineering*, Vol. 14, No. 7, 2004, pp. 1057–1063. doi:10.1088/0960-1317/14/7/028

[20] Cai, C., Sun, Q., and Boyd, I. D., "Gas Flows in Microchannels and Microtubes," *Journal of Fluid Mechanics*, Vol. 589, No. 589, Oct. 2007, pp. 305–314. doi:10.1017/S0022112007008178

[21] Nguyen, N. T., and Wereley, S. T., *Fundamentals and Applications of Microfluidics*, Artech House, Boston, 2002.

[22] Brask, A., Goranovic, G., Jensen, M. J., and Bruus, H., "A Novel Electro-Osmotic Pump Design for Nonconducting Liquids: Theoretical Analysis of Flow Rate-Pressure Characteristics and Stability," *Journal of Micromechanics and Microengineering*, Vol. 15, No. 4, 2005, pp. 883–891. doi:10.1088/0960-1317/15/4/029

[23] Patanka, N. A., and Hu, H. H., "Numerical Simulation of Electroosmotic Flow," *Analytical Chemistry*, Vol. 70, No. 9, 1998, pp. 1870–1881. doi:10.1021/ac970846u

[24] Vainshtein, P., and Gutfinger, C., "On Electroviscous Effects in Microchannels," *Journal of Micromechanics and Microengineering*, Vol. 12, No. 22, Mar. 2002, pp. 252–256. doi:10.1088/0960-1317/12/3/309

[25] Wang, J., Wang, M., and Li, Z., "Lattice Poisson-Boltzmann Simulations of Electro-Osmotic Flows in Microchannels," *Journal of Colloid and Interface Science*, Vol. 296, No. 2, 2006, pp. 729–736. doi:10.1016/j.jcis.2005.09.042

[26] Yang, R. J., and Lin, Y. C., "Electroosmotic Flow in Microchannels," *Journal of Colloid and Interface Science*, Vol. 239, No. 1, 2001, pp. 98–105. doi:10.1006/jcis.2001.7551

[27] Gao, Y., Wong, T. N., Yang, C., and Ooi, K. T., "Two-Fluid Electro-Osmotic Flow in Microchannels," *Journal of Colloid and Interface Science*, Vol. 284, No. 1, Apr. 2005, pp. 306–314. doi:10.1016/j.jcis.2004.10.011

[28] Ngoma, G. D., and Erchiqui, F., "Pressure Gradient and Electro-Osmotic Effects on Two Immiscible Fluids in a Microchannel Between Two Parallel Plates," *Journal of Micromechanics and Microengineering*, Vol. 16, Jan. 2006, pp. 83–91. doi:10.1088/0960-1317/16/1/012

[29] Boyd, T. J. M., and Sanderson, J. J., *Plasmadynamics*, Nelson, London, 1969.

[30] Agarwal, R. K., "Lattice Boltzmann Simulations of Magneto-hydrodynamics Slip Flow in Microchannels," 36th AIAA Plasmadynamics and Lasers Conference, Toronto, AIAA Paper 2005-4782, June 2005.

[31] Naterer, G. F., and Camberos, J. A., *Entropy Based Design of Thermofluid and Microfluidic Systems*, CRC Press, Boca Raton, FL, June 2007.
[32] Gaitonde, D. V., and Poggie, J., "Simulation of MHD Flow Control Techniques," Fluids Dynamics Conference, Denver, CO, AIAA Paper 2000-2326, 19–22 June 2000.
[33] MacCormack, R. W., "Simulation of Hypersonic Flow Within a Strong Magnetic Field," 45th AIAA Aerospace Sciences Conference, Reno, NV, AIAA Paper 2007-0397, Jan. 2007.
[34] Chen, X., *Gaskinetics and Its Applications in Heat Transfer and Flow*, Tsinghua Univ. Press, Beijing, 1996.
[35] Hill, P., and Peterson, C., *Mechanics and Thermodynamics of Propulsion*, 2nd ed., Addison–Wesley, Reading, MA, 1992.

X. Zhong
Associate Editor